

ON THE EVIDENCE FOR EXTREME GRAVITY EFFECTS IN MCG –6–30–15

K. A. Weaver¹ and T. Yaqoob²

ABSTRACT

We examine the unusual Fe-K α line profile in MCG –6–30–15 observed by *ASCA* during a deep minimum in the source intensity. The intense red wing and depressed blue wing of the line have been interpreted as evidence for extreme gravitational redshifts in terms of emission from within six gravitational radii of a black hole. We find that the data do not uniquely support this interpretation and can be equally well explained by occultation of the continuum source and the putative line-emitting accretion disk, which we offer as an alternative hypothesis. Two problems with previous modeling were that the equivalent width of the line during the deep minimum was required to be unusually large (> 1 keV) and the line intensity was thought to increase as the source became dim. The occultation model does not suffer from these problems. Our results serve to highlight the hazards of over-interpreting observational results which have low statistical significance, to the extent that theoretical implications can become generally accepted when the data do not provide a strong case for them.

Subject headings: black hole physics – galaxies:active –
galaxies:individual:MCG–6-30-15 – line:profiles – X-rays:galaxies

¹Department of Physics and Astronomy, Johns Hopkins University, Bloomberg Center, Baltimore, MD 21218. kweaver@pha.jhu.edu

²NASA/ Goddard Space Flight Center, Laboratory for High Energy Astrophysics, Greenbelt, MD 20771, USA.

1. Introduction

Recently, Iwasawa *et al.* (1996; hereafter I96) found an extremely broad iron $K\alpha$ emission line with a particularly prominent red wing, extending down to ~ 4 keV, during an extended observation with the *Advanced Satellite for Cosmology and Astrophysics* (*ASCA*; see Tanaka, Inoue & Holt 1994). The peculiar line profile, measured during what has been dubbed a ‘deep minimum’ (or DM) in the X-ray light curve, had much more emission in the red wing, and much less around the line rest energy (~ 6.4 keV), compared to the Fe $K\alpha$ profiles thus far measured for MCG –6–30–15 and other AGNs (e.g. Tanaka *et al.* 1995, Yaqoob *et al.* 1995, Nandra *et al.* 1997). Also, the equivalent width of the line was unusually large, of the order of ~ 1 keV, a factor of ~ 3 larger than most such measurements of broad iron K lines in Seyfert 1 galaxies. For the DM state of MCG –6–30–15, I96 rejected the standard model for the Fe- $K\alpha$ line profile (e.g. see Fabian *et al.* 1989), in which the line is emitted in an accretion disk rotating about a Schwarzschild black hole, with the inner disk extending no closer than the radius for marginally stable orbits, (i.e. 6 gravitational radii, or $6r_g$). Instead, the extreme gravitational redshifts implied by the bloated red wing of the line were explained either in terms of emission from inside the last stable orbit around a Schwarzschild hole (Reynolds & Begelman 1997) or emission in a disk rotating about a Kerr black hole (e.g. I96; Dabrowski *et al.* 1997; Bromley, Miller & Pariev 1998). In the latter case the last stable orbit extends down to $1.24r_g$ for a maximally rotating Kerr black hole. In both cases, the red wing of the line is accounted for by emission closer to the black hole event horizon, so the photons can experience the effects of very strong gravity, resulting in extremely large redshifts.

We point out that in terms of fitting the DM data for MCG –6–30–15 with the standard model (Schwarzschild hole, disk extending to $6r_g$) and the Kerr model (disk extending to $1.24r_g$), the largest difference in the fitting statistic, $\Delta\chi^2$, is 6.2 for the same number of free model parameters (see rows 1 and 3 in Table 3 of I96 who assume a disk inclination of 30° and an outer radius of $15.5r_g$). While this may be interpreted as being formally statistically significant, *ASCA* spectral fits do not in general (and in this case, in particular) include the effects of systematic errors which could reduce the overall significance of the result. Since the implications of really being able to observe X-rays inside of $6r_g$ and even closer to a black hole event horizon are so far reaching (e.g. see Fabian 1997) it is important to investigate the robustness of the result for MCG –6–30–15, the only case thus far reported.

2. ASCA Data

ASCA observed MCG –6–30–15 for over 4 days starting 1994, July 23. *ASCA* has four identical, thin-foil, light-weight X-ray telescopes (XRT) which focus X-rays onto one of two Solid-state Imaging Spectrometers (SIS) or one of two Gas Imaging Spectrometers (GIS, see Ohashi *et al.* 1991). See Tanaka *et al.* (1994) for a summary of the *ASCA* mission and focal-plane detectors. The SIS sensors, each one consisting of four CCD (charge coupled device) chips were operated in a mode in which only one chip was exposed (1-CCD mode) and the data were accumulated in FAINT mode. Hereafter the two SIS sensors are referred to as SIS0 and SIS1 and the two GIS sensors as GIS2 and GIS3. The data reduction and selection criteria are similar to those described in Yaqoob *et al.* (1994).

The lightcurve of the entire observation has been presented elsewhere (I96; Reynolds *et al.* 1997; Yaqoob *et al.* 1997). We use exactly the same time intervals defined by I96 to extract spectra of the DM state (interval $i - 7$ in their Figure 2) and the flare state (interval $i - 3$), as well as the average (total) spectrum. For the DM, we obtained 3 – 10 keV count rates in the range 0.13 to 0.16 counts s^{-1} and exposure times in the range 13.2 to 13.3 ks for the four instruments. Figure 1 shows the ratio of the data in the DM to the best-fitting power-law model ($\Gamma = 1.92$, $N_H = 1.1 \times 10^{22} \text{ cm}^{-2}$) using data only in the energy ranges 2 – 3 keV and 8 – 10 keV. The excess above the underlying power-law is due to the Fe-K α line emission. As pointed out by I96, the emission on the blue side of the line is unusually diminished compared to the red side. The portion of the lightcurve containing the DM state is shown in Figure 2.

3. Standard Disk-line Spectral Fits

Using data between 3 and 10 keV from all four instruments, we fitted the Fe-K α line for the average, flare and DM spectra with our ‘baseline’ model in which the line photons are emitted in a disk rotating around a central Schwarzschild black hole (e.g., Fabian *et al.* 1989). The parameters are θ_{obs} (inclination angle of the disk normal relative to the observer), r_i (inner disk radius), r_o (outer disk radius), q (power-law index characterizing the line emissivity as $\propto r^{-q}$), I_D (line intensity), and E_D (line energy in the disk rest frame). The inner radius, r_i , was fixed at $6r_g$ where $r_g \equiv GM/c^2$ (i.e. the last stable orbit). There is interplay between E_D and the other line parameters, so E_D was fixed at 6.4 keV in the rest frame, corresponding to fluorescence in a cold disk. The results are shown in Table 1, models SH1, SH2, and SH3.

We repeated the above fitting, but this time replacing the Schwarzschild black hole

with a maximally rotating Kerr black hole (see e.g., Laor 1991). Now the inner radius is fixed at $1.24r_g$, the minimum value, or last stable orbit for the Kerr metric. The spectral fit was repeated with E_D fixed at 6.7 keV (corresponding to He-like Fe). For the average and flare spectra, a Kerr profile does not improve the fit, but for the DM, the Kerr model provides a statistically better fit than the Schwarzschild model ($\Delta\chi^2 \sim 5$). The results for the DM are shown in Table 1, models KR1 and KR2. The basic reason why the Fe-K α line during the DM is better described by emission from matter closer than $6r_g$ is that the observed strength of the blue peak of the line is too small for the observed strength of the red wing. This is compensated by the extra gravitational redshifts obtained by placing the emitter closer to the black hole, increasing the intensity of the red wing relative to the blue. Our results confirm those of I96, although the best-fitting parameters differ slightly because we fix q at 2.5 and allow θ_{obs} and r_o to be free, the contrary to their technique.

4. Spectral Fits with an Occultation Model

We tested whether we could fit the DM Fe-K α line profile without placing line-emitting matter closer to the black hole than $6r_g$ by obscuring part of the standard Schwarzschild disk with optically-thick matter. Figure 3 illustrates how different parts of a Schwarzschild disk affect the Doppler and gravitational shift of line photons. Defining $g = E(\text{observed})/E(\text{emitted})$ (including both Doppler and gravitational effects), the shaded part labeled blue corresponds to $g > 1$ and the shaded part labeled red corresponds to $g < (1/1.2)$. In our simple-minded model, the occultation of the disk is in the form of a strip running along the x or y directions, with half-width y_0 or x_0 respectively, passing symmetrically over the center of the disk. Thus, line emission from either $|y| < y_0$ or $|x| < x_0$ is blocked from view and the predicted line profiles for the two cases are shown in Figures 4a and 4b respectively (for several values of the half-width). We use this model as a hypothesis, since we do not know the geometry of the optically-thick clouds (there are plenty of arguments for their existence, e.g. Guilbert & Rees 1988). The clouds could be spherical, filament-shaped, or neither. Our simple model in some sense mimics an optically-thick cloud, whatever its shape, moving over the disk, resulting in some kind of average line profile. Clearly, the profiles in Figure 4a, in which much of the blueshifted emission is obscured, are relevant for the DM data.

For the spectral fits with the obscuration model, we fix $E_D = 6.4$ keV and $r_i = 6r_g$ as before, and $r_o = 18.5r_g$ from the Schwarzschild fit (Table 1, SH3). The best-fitting parameters are shown in Table 1, model OC1. This fit is marginally better than the Kerr model with $E = 6.4$ keV (model KR1) and marginally worse than the Kerr model with

$E = 6.7$ keV (model KR2) and so we conclude that the occulted, Schwarzschild disk-line model describes the spectrum during the DM just as well as the standard Kerr model.

The above fits include only Galactic absorption because we assume that there is no significant absorption from the ‘warm absorber’ present above 3 keV that will affect the shape of the continuum (Fabian *et al.* 1994; Reynolds *et al.* 1995; Otani *et al.* 1996). This was also the assumption made by I96 and is based on observations of the warm absorber in MCG–6-30-15 in higher flux states. However, if absorption were present, this could also affect measurements of the Fe-K α line. Figure 5 shows the data/model ratio when the DM spectrum is fitted with Galactic absorption and a power law with the best-fitting photon index of the average spectrum ($\Gamma = 1.98$). The deficiency of low-energy photons due to the ionized absorber is significant, even *above* 3 keV, and implies that the flattening of the continuum in the DM (Table 1, models SH3, KR1, KR2, OC1) is due to absorption. Thus, the *intrinsic* spectral slope during the DM is not required to change.

We therefore fitted the DM spectrum again with the occultation-line model with Γ fixed at the average value of $\Gamma = 1.98$, but with free absorption (Table 1, model OC2). The number of free parameters is the same as before, but $\Delta\chi^2 = 5.7$ compared to the best-fitting Kerr model (model KR2). The occultation description of the DM is thus as viable as the scenarios posited by I96, Reynolds & Begelman (1997), Dabrowski *et al.* (1997), and Bromley *et al.* (1998).

5. Discussion and Conclusions

We have examined the Fe-K α line profile during the deep minimum (DM) flux state for MCG–6-30-15 with an ‘occultation model’ in which the continuum source and much of the blueshifted part of the emission from the disk is obscured by an optically-thick cloud. This model describes the observed line profile as well as the Kerr black-hole/disk model, but does not require emission from inside $6r_g$ (the last stable orbit for a Schwarzschild black hole). One difficulty with the Kerr interpretation proposed by I96 and others is that it doesn’t explain why Kerr effects should only manifest themselves in the DM. The occultation model does not suffer from this problem. Also, the line intensity is *not* required to increase relative to the average line intensity, as has been previously claimed. Nor is the equivalent width (EW) of the Fe-K line during the DM required to be unusually large. We obtain $EW \sim 400$ eV for the DM *and* flare-states, and $EW \sim 470$ eV for the average line.

In addition to the optically-thick obscurer that blocks most of the continuum region, the data above 3 keV are affected by the O VIII edge of the warm absorber that becomes

stronger in the low-flux state (Otani *et al.* 1996). We measure an additional column density of $\sim 2 \times 10^{22} \text{ cm}^{-2}$ in the DM, which is a factor of ~ 2 increase compared to the high flux state (Fabian *et al.* 1994). The increase in column density is consistent with a picture in which the material that is photoionized by the central source becomes less opaque to soft X-rays due to a reduction in ionization when the continuum is blocked. Note that the extra absorption we directly measure is *not* necessarily related to the optically-thick clouds responsible for obscuring the Fe-K α line emission.

To conclude, we have shown that the unusual Fe-K α line profile in MCG –6–30–15 during a deep minimum in intensity does not necessarily require line emission from within $6r_g$ and that the data are not adequate enough to distinguish between the Schwarzschild and Kerr solutions. Sulentic *et al.* (1998) have also made the suggestion that a Kerr black hole is not required, proposing that the true shape of the Fe-K α line is a double Gaussian, but offer no physical model. We have shown that the deep-minimum line profile can be explained by occultation of a standard Schwarzschild disk. This model is consistent with the detailed temporal profile of the continuum intensity dip. Our results serve to highlight the hazards of over-interpreting observational results which have low statistical significance, to the extent that theoretical implications can become generally accepted when the data do not provide a strong case for them.

REFERENCES

- Bromley, B. C., Miller, W. A., & Pariev, V. I. 1998, *Nature*, 391, 54
- Dabrowski, Y., Fabian, A. C., Iwasawa, K., Lasenby, A. N., & Reynolds, C. S. 1997, *MNRAS*, 288, L11
- Fabian, A. C., Rees, M. J., Stella, L., & White, N. E. 1989, *MNRAS*, 238, 729
- Fabian, A. C., *et al.* 1994, *PASJ*, 46, L59
- Fabian, A. C. 1997, *A&G*, 38, 10
- Guilbert, P. W., & Rees, M. J. 1988, *MNRAS*, 233, 475
- Iwasawa, K., *et al.* 1996, *MNRAS*, 282, 1038
- Laor, A. 1991, *ApJ*, 376, 90
- McKernan, B., & Yaqoob, T. 1998, *ApJ*, in press astro-ph/9804265
- Nandra, K., George, I. M., Mushotzky, R. F., Turner, T. J. , & Yaqoob, T. 1997, *ApJ*, 476, 70
- Ohashi, T. *et al.* 1991, *Proc. SPIE*, 1549, 9
- Otani, C. *et al.* 1996, *PASJ*, 48, 211
- Reynolds, C S., Fabian, A. C., Nandra, K., Inoue, H., Kunieda, H., & Iwasawa, K. 1995, *MNRAS*, 277, 901
- Reynolds, C. S., & Begelman, M. C. 1997, *ApJ*, 488, 109
- Sulentic, J. W., Marziani, P., Zwitter, T., Calvani, M., Dultzin-Hacyan, & D. 1998, *ApJ*, in press, astro-ph/9712336
- Tanaka, Y., Inoue, H., & Holt, S. S. 1994, *PASJ*, 46, L37
- Tanaka, Y., *et al.* 1995, *Nat*, 375, 659
- Yaqoob, T., Serlemitsos, P. J., Mushotzky, R. F., Madejski, G., Turner, T.J., & Kunieda, H. 1994, *PASJ*, 46, L173
- Yaqoob, T., Edelson, R., Weaver, K. A., Warwick, R. S., Mushotzky, R. F., Serlemitsos, P. J., & Holt, S. S. 1995, *ApJ*, 453, L81
- Yaqoob, T., McKernan, B., Ptak, A., Nandra, K., Serlemitsos, P. J. 1997, *ApJ*, 490, L25

Table 1. MCG–6-30-15: Relativistic Disk-Model Spectral Fits (3 – 10 keV) for the Fe K α line¹.

Data set	Model ²	Γ	r_o/r_g	θ_{obs} (degrees)	I_{Fe} ³	EW (eV)	y_0/r_g	χ^2/ν
Average	SH1	$1.98^{+0.04}_{-0.04}$	$15.6^{+5.7}_{-4.4}$	$33.7^{+1.8}_{-1.9}$	$1.88^{+0.30}_{-0.31}$	473^{+75}_{-78}	...	1417.9/1355
Flare	SH2	$2.00^{+0.07}_{-0.06}$	$6.1^{+2.0}_{-0.01\dagger}$	$39.4^{+2.4}_{-6.5}$	$2.29^{+0.78}_{-0.80}$	410^{+142}_{-140}	...	925.6/899
Deep Min.	SH3	$1.71^{+0.17}_{-0.17}$	$18.5^{+19.4}_{-9.3}$	27^{+10}_{-10}	$1.52^{+0.74}_{-0.68}$	665^{+324}_{-298}	...	305.2/323
Deep Min.	KR1	$1.73^{+0.19}_{-0.17}$	$19.8^{+30.0}_{-18.56\dagger}$	31^{+39}_{-12}	$2.28^{+1.04}_{-0.95}$	1070^{+488}_{-446}	...	299.6/323
Deep Min.	KR2 ⁴	$1.73^{+0.21}_{-0.18}$	$13.3^{+15.4}_{-12.06\dagger}$	27^{+39}_{-10}	$2.42^{+1.22}_{-1.04}$	1130^{+570}_{-486}	...	297.6/323
Deep Min.	OC1 ⁵	$1.74^{+0.20}_{-0.17}$	18.5f	46^{+43}_{-23}	$1.63^{+1.07}_{-0.71}$	481^{+316}_{-210}	$8.0^{+4.1}_{-8.0}$	298.2/323
Deep Min.	OC2 ^{5,6}	1.98f	18.5f	51^{+38}_{-24}	$1.53^{+0.78}_{-0.76}$	404^{+206}_{-201}	$8.8^{+4.1}_{-7.2}$	291.9/323

¹Errors are 90% confidence for 4 interesting parameters ($\chi^2 + 7.78$). Fixed parameters are denoted by ‘f’. The center energy of the iron line in the disk frame is fixed at 6.4 keV unless otherwise stated. $N_{\text{H}}(\text{Gal.}) = 5 \times 10^{20} \text{ cm}^{-2}$ is assumed for all fits.

²Theoretical models for the iron line are SH: Schwarzschild profile, KR: Kerr profile, OC: occulted, Schwarzschild disk-line model.

³Line intensity in units $10^{-4} \text{ photons cm}^{-2} \text{ s}^{-1}$. Intensities and equivalent widths (EW) are in the *observed* frame.

⁴The iron line center energy in this Kerr model is fixed at 6.7 keV in the disk frame.

⁵The occulted disk model is described in the text. The parameter y_0 is the half-width of an obscuring strip running symmetrically over the center of the disk (see Figure 3).

⁶In this model there is an additional absorbing column with $N_{\text{H}} = 1.96^{+1.29}_{-1.31} \times 10^{22} \text{ cm}^{-2}$.

[†]The lower bounds on r_o for these fits are not true statistical errors but represent the radius of last stable orbit around a maximally rotating Kerr black hole ($1.235r_g$).

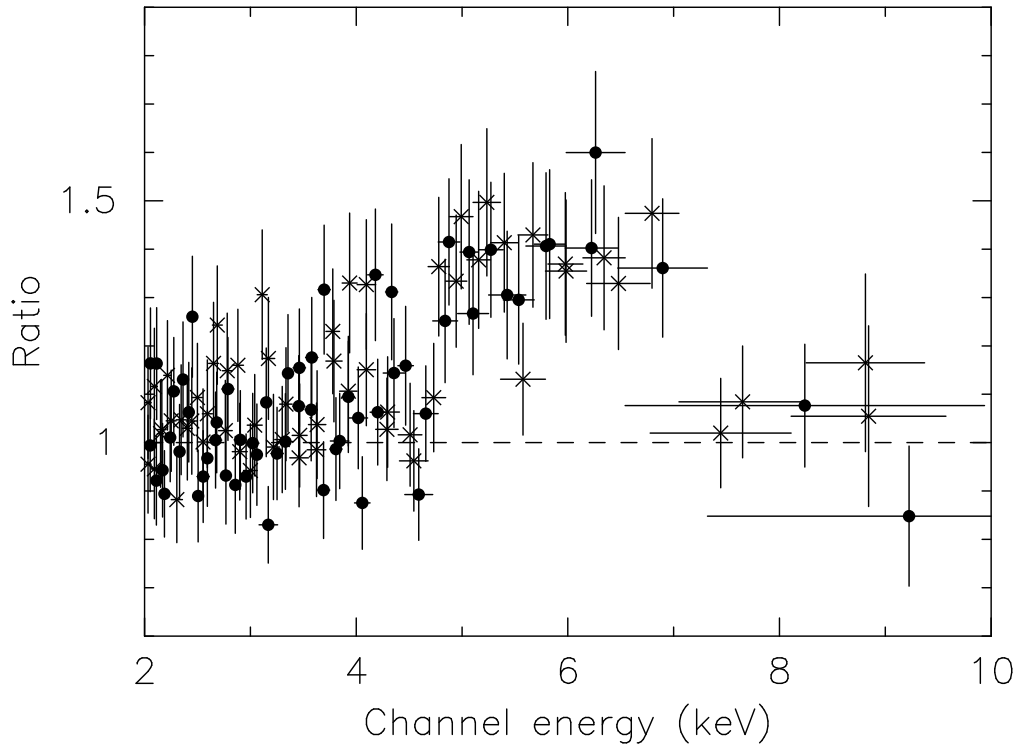


Figure 1

Fig. 1.— Ratio of the *ASCA* data (all detectors) from the deep minimum to a continuum model that consists of the best-fitting absorbed power law. The data between 3 and 8 keV were ignored for the fit. Filled circles correspond to SIS0 and SIS1 data and crosses correspond to GIS2 and GIS3 data.

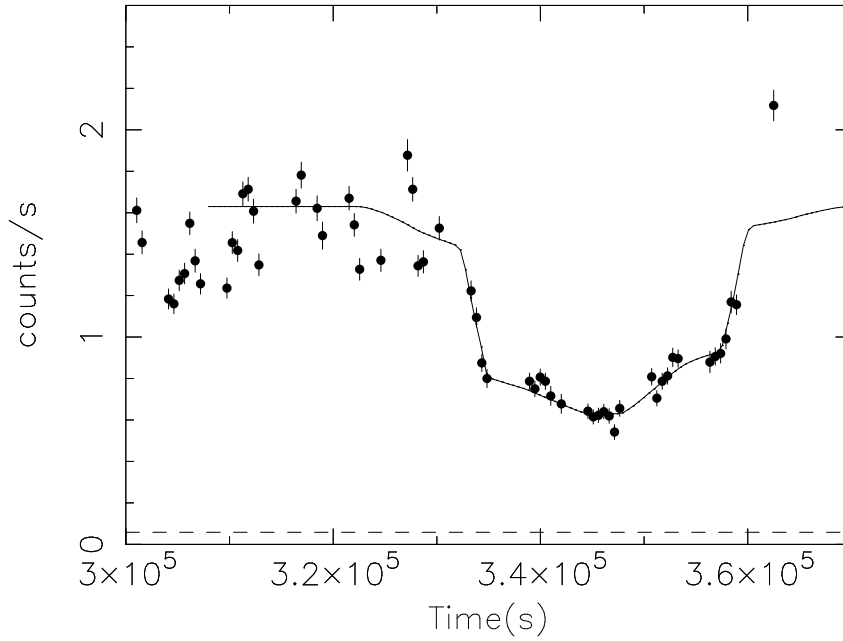


Fig. 2.— The deep minimum (DM) light curve with the model from McKernan and Yaqoob (1998) in which the temporal profile of the DM lightcurve can be explained by an obscuring body passing over the disk and central source. To explain the temporal data, the part of the disk for which the emission is blueshifted must be occulted first, and it remains occulted for a large part of the duration of the intensity dip. The dashed line is the mean background level.

Figure 2

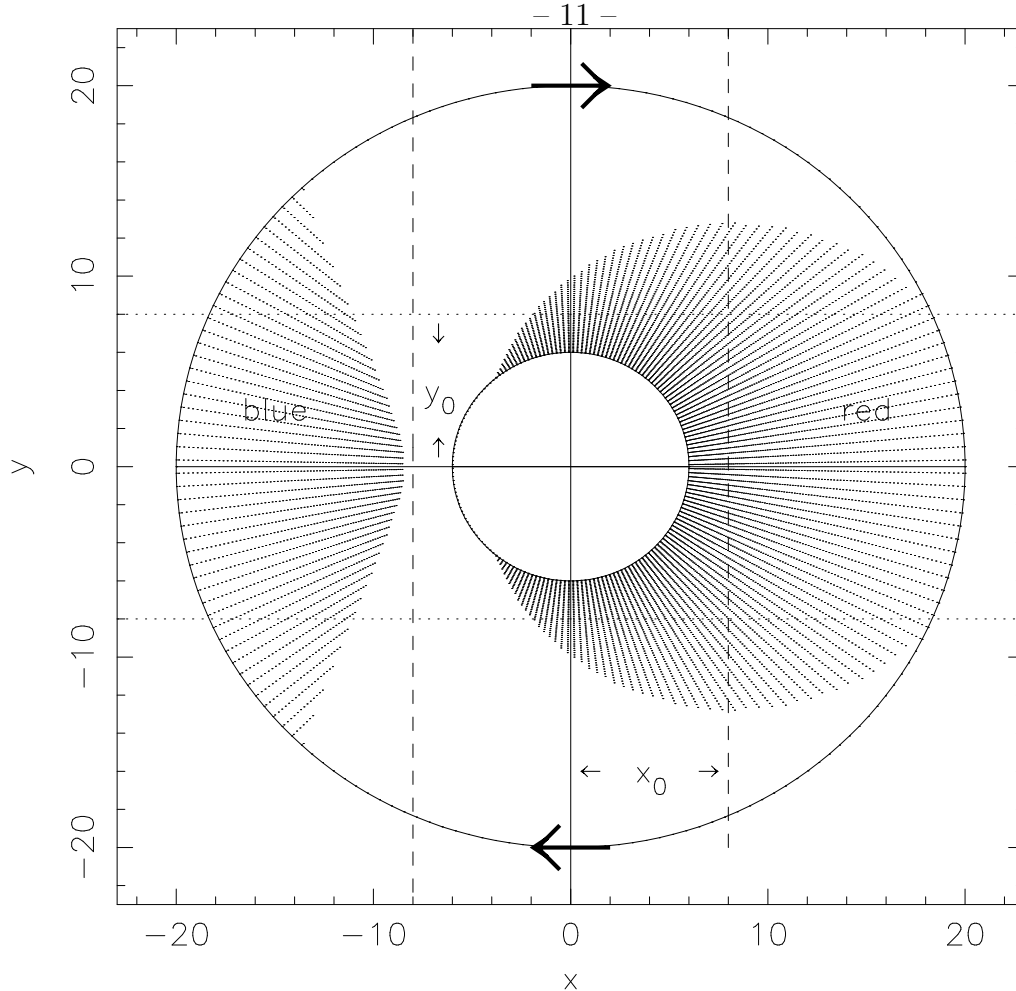


Fig. 3.— Illustration of how different parts of the Schwarzschild disk affect the Doppler and gravitational shift of line photons. Defining $g = E(\text{observed})/E(\text{emitted})$ (including both Doppler and gravitational effects), the shaded part labeled blue corresponds to $g > 1$ and the shaded part labeled red corresponds to $g < (1/1.2)$. The obscuration model is such that lines-of-sight to the region inside $|x| < x_0$ or $|y| < y_0$ are blocked from view (see text). In this diagram the disk is inclined at 30° , such that the disk normal is pointing downwards towards the negative y axis. The inner and outer disk radii are $r_i = 6r_g$ and $r_o = 20r_g$.

Figure

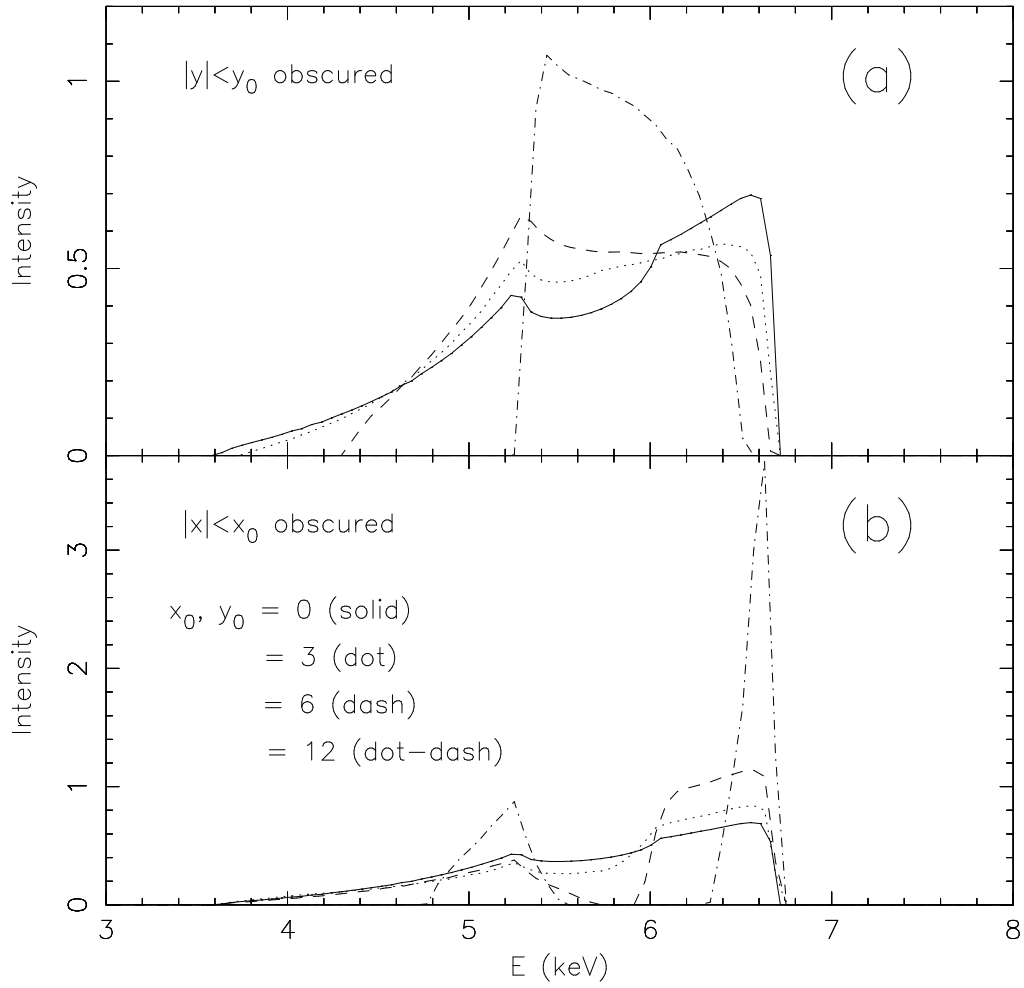


Fig. 4.— Theoretical calculations of the iron line profile from an obscured Schwarzschild disk with the dimensions of the obscurer (x_0 and y_0) as shown and the remaining parameters as in Figure 3.

Fig. 4

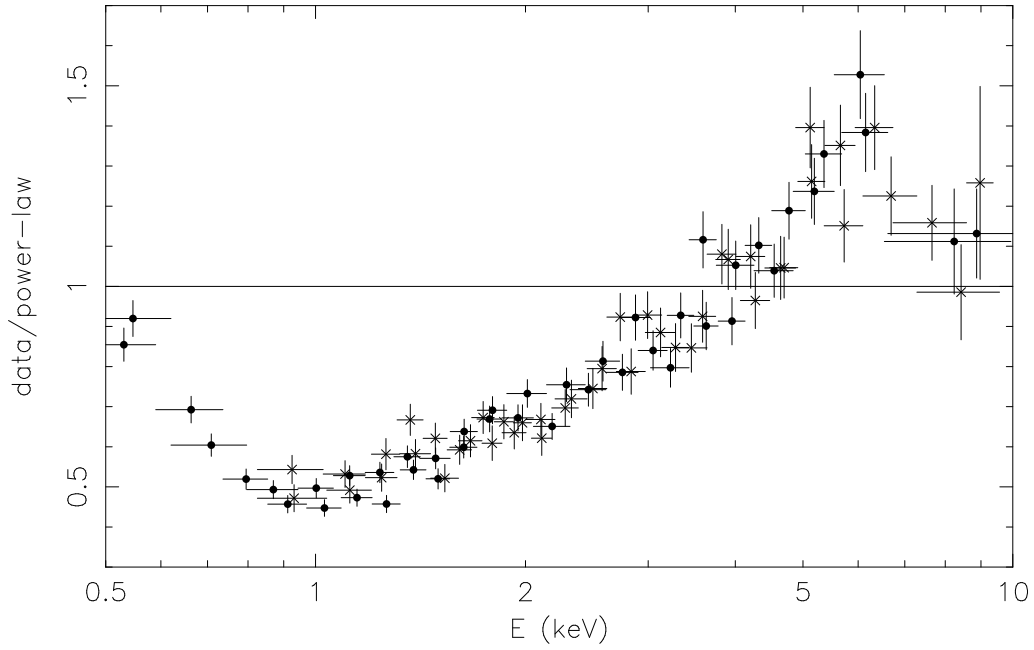


Fig. 5.— Ratio of the data to model when the deep minimum spectra (from the four *ASCA* instruments) are fitted with only Galactic absorption and a power law with the slope fixed at the value obtained from the average 4.2-day spectrum (i.e., $\Gamma = 1.98$, see model SH1 in Table 1). The extra absorption during the deep minimum is clearly evident, even above 3 keV. Filled circles correspond to SIS0 and SIS1 data and crosses correspond to GIS2 and GIS3 data.

Figure 5